ELSEVIER

Physics of the Earth and Planetary Interiors 130 (2002) 17–29

PHYSICS OF THE EARTH AND PLANETARY INTERIORS

www.elsevier.com/locate/pepi

Determination of focal mechanism solution using initial motion polarity of P and S waves

Masaki Nakamura*

Meteorological Res. Inst., Japan, Nagamine 1-1, Tsukuba, Ibaraki-ken 3050052, Japan

Received 6 October 2000; received in revised form 24 July 2001; accepted 6 November 2001

Abstract

It is important to determine accurate focal mechanism solutions for earthquakes with small magnitudes or those recorded by a small number of seismometers, perhaps with an unfavorable geographic distribution. A method using initial motion polarity of S waves, in addition to P waves, is described. This method can be applied routinely to determine the focal mechanism solution of earthquakes which occur all over Japan where a nationwide earthquake observation network of high sensitivity seismographs at a few tens of kilometers interval will soon be available. We define Q to be a weighted sum of inconsistencies between observed and calculated polarities. Double-couple focal mechanisms are searched to determine the solution that produces the smallest misfit $Q_{\min}$, and the set of acceptable mechanisms: $Q \leq Q_{\min} + 1.5$. The uncertainty of each principle axis is expressed as the maximum angle between the best solution and all the acceptable solutions.

Keywords: Focal mechanism; Initial S polarity; Reliability; High sensitivity seismograph

1. Introduction

Determining the focal mechanisms of many earthquakes, which are not only large but also small or micro, with sufficient accuracy, contributes to an evaluation of the state of the crustal stress. Now, Japan Meteorological Agency (JMA) determines the focal mechanism solution using the initial motion polarity of P waves recorded by high sensitivity seismographs. Moreover, it determines CMT solution of relatively large earthquakes (magnitudes larger than 5) using waveforms recorded by broadband seismographs. On the other hand, national organization like Japanese Ministry of Education, Culture, Sports, Science and Technology will establish a nationwide earthquake observation network by deploying high sensitivity seismographs with a spacing of a few tens of kilometers. On the basis of these, I propose a method to determine the focal mechanism solution of many earthquakes efficiently, using waveforms observed by this high sensitivity seismograph network all over Japan.

Using waveforms recorded by high sensitivity seismographs, in addition to the method using the initial motion polarity of P waves, various methods have been proposed by many authors to determine the focal mechanism solutions. Stauder and Bollinger (1964), Hirasawa (1970), Kisslinger (1980), Julian and Foulger (1996), Rau et al. (1996) and Nakamura et al. (1999) used the ratio of amplitudes of P, SV, and SH waves, and Ito et al. (1998) the whole waveforms. However, in these methods, because of the scattering of seismic waves, the observed value is not consistent with the theoretical, especially in the case of small earthquakes, so it is thought that the observation

* Tel.: +81-298-52-9361; fax: +81-298-51-3730.
E-mail address: mnakamur@mri-jma.go.jp (M. Nakamura).

0031-9201/02/$ – see front matter
PII: S0031-9201(01)00306-5

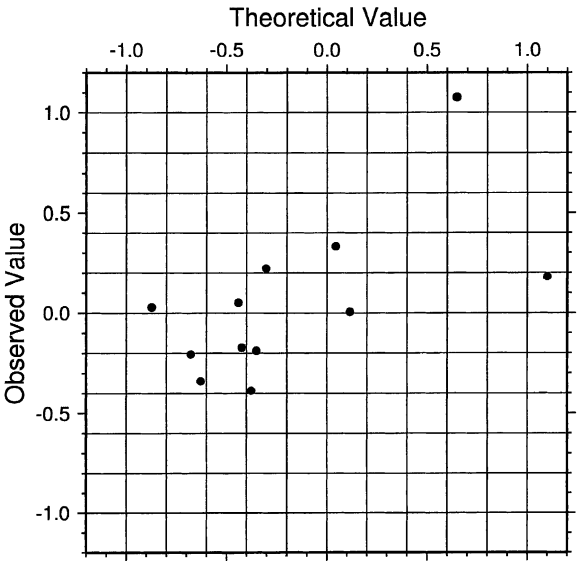

Fig. 1. The result of the simple examination, how consistent the observed ratio of amplitudes is with the theoretical ones without any kinds of corrections, assuming the focal mechanism solutions which are determined much stably only with initial motion polarity of P waves. This is a case where epicentral distance is limited less than 200 km, hypocenters are limited deeper than 250 km and the plotted value is in logarithmic scale, i.e. log ((amplitude of SV)–(amplitude of SH)). In this example, the observed values are not consistent with the theoretical ones, but it is better than other examples.

stations usable for the analysis are limited to those close to the hypocenter without any kinds of correction. Fig. 1 shows a result of the simple examination of the above. In this example, the observed values are not consistent with the theoretical ones, but it is better than other examples. Therefore, it is questionable to apply these methods routinely to the seismograph network of a few tens of kilometers interval.

In this study, I propose a method to determine the focal mechanism solution using the initial motion polarities of S waves, which are not easily affected by path effect etc., like that of P waves. Here, the initial motion polarity of S waves, for example, in the case of seismic waves in Fig. 2, is South for NS component, and is West for EW component, as it is Up for P wave. The method is available in the recent version of computer program FOCMEC (Snoke et al. (1984)), but its effectiveness has not been discussed. Therefore, I apply this method to some Japanese earthquakes

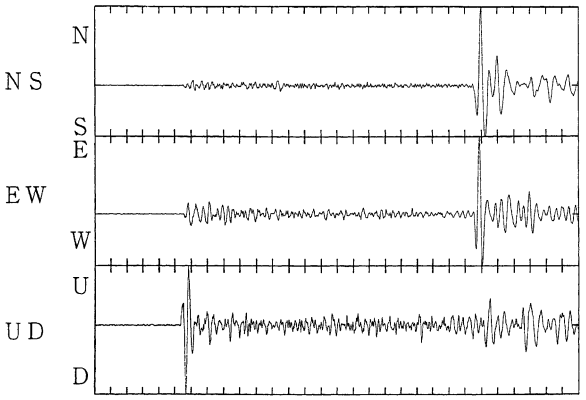

Fig. 2. The common seismogram. In this example, initial motion polarity of the S wave is South for NS component, and is West for EW component.

and show its effectiveness. Furthermore, I examine the method to display a focal mechanism solution including information concerning the observation stations, and present a formula to express the reliability of the focal mechanism solution.

2. Method

I introduce the double couple model as a point source model, and introduce the focal sphere of a unit radius. Where the unit vectors in the direction of two couple of forces, null axis, pressure axis, and tension axis are $\vec{A}$, $\vec{B}$, $\vec{N}$, $\vec{P}$, and $\vec{T}$, respectively,

$$\begin{aligned} &(\vec{P}\cdot\vec{T}) = 0 \\ &\vec{A} = \frac{(\vec{P}+\vec{T})}{\sqrt{2}} \\ &\vec{B} = \frac{(-\vec{P}+\vec{T})}{\sqrt{2}} \\ &\vec{N} = (\vec{A}\times\vec{B}) = (\vec{P}\times\vec{T}) \end{aligned} \tag{1}$$

Here, I give the method to calculate $\vec{A}$, $\vec{B}$, $\vec{N}$, $\vec{P}$, and $\vec{T}$ which satisfy the observed initial motion polarity of P and S waves.

I introduce the coordinate system shown in Fig. 3. Moreover, I introduce a focal mechanism solution with strike ϕ_s, dip angle ν, and slip angle λ as one of the nodal plane. When a ray radiates to focal sphere with take-off angle δ, azimuth ϕ, the direction of P wave

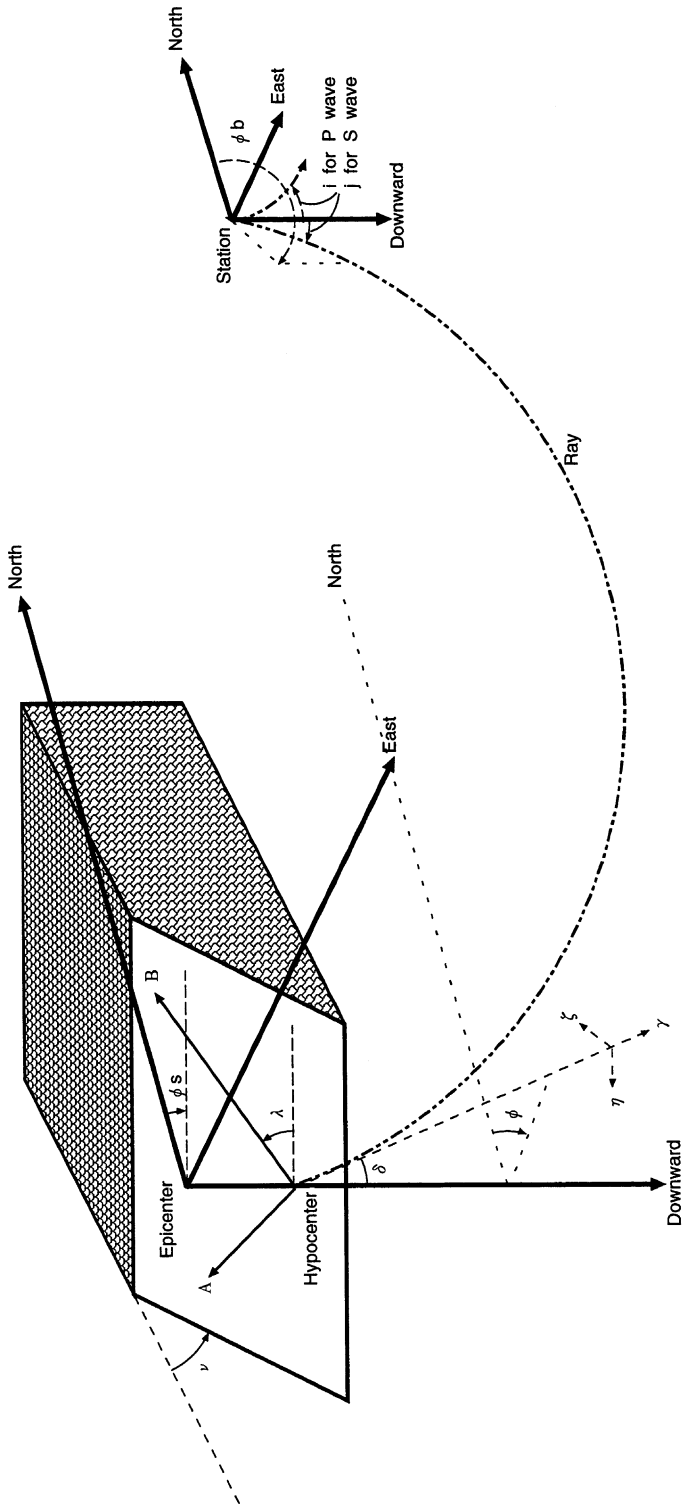

Fig. 3. The definition of the coordinate system.

motion $\vec{\gamma}$, the direction of SV wave motion $\vec{\zeta}$, and the direction of SH wave motion $\vec{\eta}$, the position of station is $\vec{\gamma}$, then the theoretical radiation pattern of P wave R_p, that of SV wave $R_{\rm sv}$, and that of SH wave $R_{\rm sh}$ are given by following equations (Aki and Richards, 1980, pp. 115):

$$
\begin{aligned}
R_p &= 2(\vec{\gamma}\cdot\vec{A})(\vec{\gamma}\cdot\vec{B}) = \cos\lambda\sin\nu\sin^2\delta\sin 2(\phi-\phi_{\rm s}) - \cos\lambda\cos\nu\sin 2\delta\cos(\phi-\phi_{\rm s}) \\
&\quad + \sin\lambda\sin 2\nu(\cos^2\delta - \sin^2\delta\sin^2(\phi-\phi_{\rm s})) + \sin\lambda\cos 2\nu\sin 2\delta\sin(\phi-\phi_{\rm s}) \\
R_{\rm sv} &= (\vec{\gamma}\cdot\vec{A})(\vec{B}\cdot\vec{\zeta}) + (\vec{\gamma}\cdot\vec{B})(\vec{A}\cdot\vec{\zeta}) = \sin\lambda\cos 2\nu\cos 2\delta\sin(\phi-\phi_{\rm s}) - \cos\lambda\cos\nu\cos 2\delta\cos(\phi-\phi_{\rm s}) \\
&\quad + \frac{\{\cos\lambda\sin\nu\sin 2\delta\sin 2(\phi-\phi_{\rm s}) - \sin\lambda\sin 2\nu\sin 2\delta(1+\sin^2(\phi-\phi_{\rm s}))\}}{2} \\
R_{\rm sh} &= (\vec{\gamma}\cdot\vec{A})(\vec{B}\cdot\vec{\eta}) + (\vec{\gamma}\cdot\vec{B})(\vec{A}\cdot\vec{\eta}) = \cos\lambda\cos\nu\cos\delta\sin(\phi-\phi_{\rm s}) \\
&\quad + \cos\lambda\sin\nu\sin\delta\cos 2(\phi-\phi_{\rm s}) + \sin\lambda\cos 2\nu\cos\delta\cos(\phi-\phi_{\rm s}) - \frac{\{\sin\lambda\sin 2\nu\sin\delta\sin 2(\phi-\phi_{\rm s})\}}{2}
\end{aligned}
\tag{2}
$$

where V_p and $V_{\rm s}$ are velocity of P and S waves near the surface (observation station), respectively, and $p = (\sin i/V_p) = (\sin j/V_{\rm s})$ is the ray parameter (Aki and Richards, 1980, pp. 140–141).

Moreover, when $\phi_{\rm b}$ is the back azimuth from the observation station to the epicenter, $R_{\rm ns}$ is the NS component of the theoretical radiation of S wave at the observation station, and $R_{\rm ew}$ is the EW component,

$$
\begin{aligned}
R_{\rm ns} &= \cos\phi_{\rm b}\cdot R_{\rm sv} + \sin\phi_{\rm b}\cdot R_{\rm sh} \\
R_{\rm ew} &= \sin\phi_{\rm b}\cdot R_{\rm sv} - \cos\phi_{\rm b}\cdot R_{\rm sh}
\end{aligned}
\tag{4}
$$

Here, when we observe P wave initial motion only with vertical component, and observe S wave initial motion only with horizontal components,

$$
\begin{aligned}
R_p &= 2\cos i(\vec{\gamma}\cdot\vec{A})(\vec{\gamma}\cdot\vec{B}) \\
R_{\rm sv} &= \cos j\{(\vec{\gamma}\cdot\vec{A})(\vec{B}\cdot\vec{\zeta}) + (\vec{\gamma}\cdot\vec{B})(\vec{A}\cdot\vec{\zeta})\} \\
R_{\rm sh} &= (\vec{\gamma}\cdot\vec{A})(\vec{B}\cdot\vec{\eta}) + (\vec{\gamma}\cdot\vec{B})(\vec{A}\cdot\vec{\eta})
\end{aligned}
$$

where i and j are angle of incidence of P wave, that of S wave, respectively. Usually, an observation station is near the surface and is influenced by the wave reflected by the free surface. When this effect is taken into consideration,

$$
\begin{aligned}
R_p &= 2(\cos i - PP\cos i + PS\sin j)(\vec{\gamma}\cdot\vec{A})(\vec{\gamma}\cdot\vec{B}) \\
R_{\rm sv} &= (\cos j + SP\sin i + SS\cos j) \\
&\quad \times\{(\vec{\gamma}\cdot\vec{A})(\vec{B}\cdot\vec{\zeta}) + (\vec{\gamma}\cdot\vec{B})(\vec{A}\cdot\vec{\zeta})\} \\
R_{\rm sh} &= 2\{(\vec{\gamma}\cdot\vec{A})(\vec{B}\cdot\vec{\eta}) + (\vec{\gamma}\cdot\vec{B})(\vec{A}\cdot\vec{\eta})\}
\end{aligned}
\tag{3}
$$

where i is the angle of P wave reflection, j that for SV wave, and

$$
\begin{aligned}
{\rm PP} &= \frac{-((1/V_{\rm s}^2)-2p^2)^2 + 4p^2(\cos i/V_p)(\cos j/V_{\rm s})}{+((1/V_{\rm s}^2)-2p^2)^2 + 4p^2(\cos i/V_p)(\cos j/V_{\rm s})} \\
{\rm PS} &= \frac{4(V_p/V_{\rm s})p(\cos i/V_p)((1/V_{\rm s}^2)-2p^2)}{((1/V_{\rm s}^2)-2p^2)^2 + 4p^2(\cos i/V_p)(\cos j/V_{\rm s})} \\
{\rm SP} &= \frac{4(V_{\rm s}/V_p)p(\cos j/V_{\rm s})((1/V_{\rm s}^2)-2p^2)}{((1/V_{\rm s}^2)-2p^2)^2 + 4p^2(\cos i/V_p)(\cos j/V_{\rm s})} \\
{\rm SS} &= \frac{((1/V_{\rm s}^2)-2p^2)^2 - 4p^2(\cos i/V_p)(\cos j/V_{\rm s})}{((1/V_{\rm s}^2)-2p^2)^2 + 4p^2(\cos i/V_p)(\cos j/V_{\rm s})}
\end{aligned}
$$

The reason I consider the initial motion polarity of NS and EW components of S wave, in addition to those of SH and SV components, is that I take into account the analysis of analog seismic waves recorded in the past, which are not easily converted to radial and transverse components.

Moreover, from Snell's law, we can calculate the angle of incidence of P wave i in Eq. (3) as follows

$$
\frac{\sin\delta}{V_{\rm src}} = \frac{\sin i}{V_p}
$$

where $V_{\rm src}$ is the P wave velocity near the source. We can calculate that of S wave j in the same way.

In this study, I assume that $V_p = 2.5$ and $V_{\rm s} = 1.5$, and calculate $V_{\rm src}$ from standard velocity structure of JMA (83A) (Hamada, 1984).

In this case, the signs of R_p, $R_{\rm sv}$, and $R_{\rm sh}$ in Eq. (2) are the same as those in Eq. (3). So, we can use Eq. (2) for simplicity. Furthermore, in these calculations, the angles of incidence do not exceed the critical angle.

Let O_i represent the observed value of initial motion polarity of P or S wave at each station, R_i the theoretical value of the same, given by Eqs. (2) and (4), and W_i the weight of each observed value, the weighted sum $\hat{Q}$ of the number of mismatches

between observed and theoretical polarities is expressed by

$$\hat{Q} = \sum_i W_i \cdot H(-\mathrm{sgn} R_i \cdot \mathrm{sgn} O_i) \quad (5)$$

where H is unit step Heaviside function, and sgn is a function, which gives the sign of the argument. $\hat{Q}$ is defined for every focal mechanism solution. Now, I deal with $\hat{Q}$ separately for each axis of focal mechanism solution. That is, I define Q, which is a function of the position on the focal sphere, as minimum value of $\hat{Q}$ for each axis of focal mechanism solution.

Let $Q_{\min}$ represent the minimum value of Q, the area of $Q_{\min}$ usually ranges over certain area on the focal sphere. However, we usually assign a certain value to each axis of focal mechanism solution for simplicity. The center of the area is adequate to each axis of focal mechanism solution. The actual procedure in this study to determine focal mechanism solution is the following: At first, P axis is assigned to the center of the area where $Q = Q_{\min}$ for P axis. Then, T axis is assigned to the center of the area where $Q = Q_{\min}$ for T axis, with the constrained condition that T axis is perpendicular to P axis. Here, it is possible to permute P and T axes.

Generally, we judge subjectively with what degree of reliability the focal mechanism solution is determined. It is based on the degree of agreement of the observed initial motion polarity with the theoretical one, calculated from the determined focal mechanism solution, so-called score, the number of observation stations, the distribution of observation stations on the focal sphere, and so on. However, it is convenient if there is an index with which we can judge the reliability of the focal mechanism solution objectively. For example, if we can determine focal mechanism solutions of many earthquakes with this index, we can statistically evaluate the state of the crustal stress field. Many methods have been proposed to express the reliability of focal mechanism solution (for example, Nakamura and Mochizuki (1988)), but generally, these methods have not been accepted widely.

The initial motion of each seismic wave is not always clear. So, it is necessary to consider the possibility of picking up a wrong polarity. If this observed value happens to be a key, which is important to provide constraints, the area of $Q_{\min}$ actually becomes wider. Therefore, we should not determine the reliability of focal mechanism solution only based on the area where Q becomes minimum.

Nakamura and Mochizuki (1988) showed that it is adequate to express the reliability of focal mechanism solution by solid angle where the size of observed data which is inconsistent with the theoretical value is between the minimum and the minimum plus 1, meaning an area of uncertainty for each axis of focal mechanism solution on focal sphere. However, solid angle can not always express the reliability adequately as in the case there is a separated isolated area in the area of uncertainty.

In this article, I propose a method to express the reliability by maximum center angle for each axis, viewed from the center of the focal sphere, between focal mechanism solution and the area of uncertainty, where $Q_{\min} \leq Q \leq Q_{\min} + \epsilon$ is searched for each axis of solution over the focal sphere (see Fig. 4). Here, I consider not only the case $Q = Q_{\min}$ but also the case $Q_{\min} \leq Q \leq Q_{\min} + \epsilon$, taking into consideration the possibility of wrong data ϵ in the observed key initial motion polarity data. Focal mechanism solution has 5 typical axes, P, T, N, A and B, so we can deal with 5 maximum center angles as the reliability. If you want to evaluate focal mechanism solution, it is a good idea to deal with the maximum value among 5 maximum center angles as the reliability. On the other hand, if you want to evaluate the crustal stress field, it is enough to deal with the maximum center angles of P and T axes as the reliability.

Usually, we show the focal mechanism solution by lower or upper hemisphere equal area projection of each axis and each nodal plane of solution on the focal sphere. Then there is a symmetric relationship with respect to the center of the circle obtained by the equal area projection of the focal sphere, between the figure obtained by the upper hemisphere of the projection and the figure obtained by the lower hemisphere of the projection. Moreover, on observed initial motion polarity of P waves, the radiation pattern has similarly a symmetric relationship, so for example, when we use the lower hemisphere of the projection, we plot the station, for which the seismic wave radiates from hypocenter downward, on the lower hemisphere of the projection, and plot the station, for which the seismic wave radiates from hypocenter upward, by projecting to the upper hemisphere and rotating 180 degree with respect to the center.

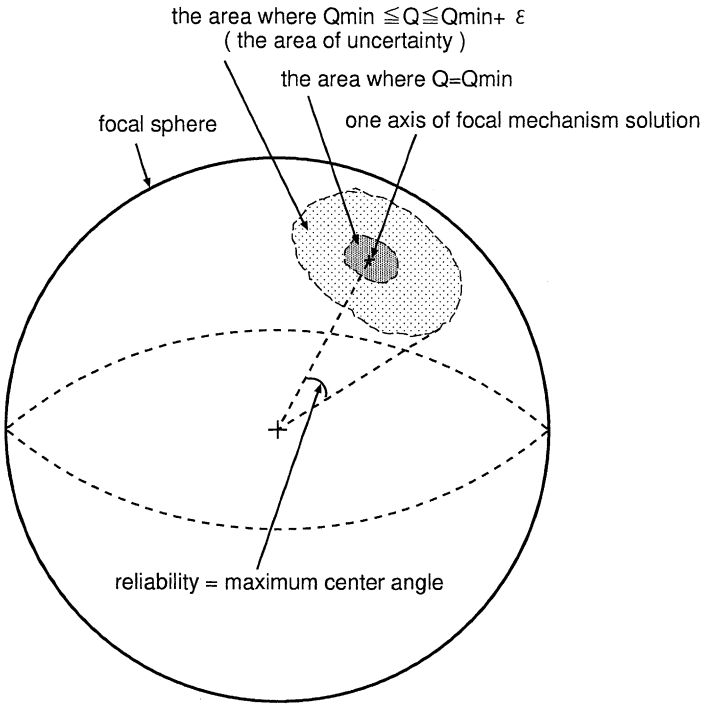

Fig. 4. The definition of the reliability.

However, the radiation pattern of the initial motion polarity of S waves does not have such a symmetric relationship except for that of SH component. In Fig. 5(b), I show the radiation pattern of the initial motion polarity of S waves of the earthquake, whose mechanism solution is shown in Fig. 5(a). Colored area, including the black one, is considered to be observed with north, east, and plus, respectively.

On the other hand, it is an important information at which position the observed values of initial motion polarity of S waves, are on the focal sphere. Therefore, in plotting the observed values of initial motion polarity of P and S waves at the same observation station near each other, I propose the following (see Fig. 5(a)): Plot the initial motion polarity of S waves like that of P waves. We distinguish the initial motion polarity by symbols. If possible, we distinguish by colors between the stations for which seismic wave radiates from the hypocenter upward and downward.

3. Discussion

I extracted 29 earthquakes, whose mechanism solution is determined with a sufficient stability with the initial motion polarity of P waves interpreted by JMA, and which occurred from April 1995 to March 1997. Hypocenter distribution map of these earthquakes is shown in Fig. 6. The reliability (maximum center angle between each axis of focal mechanism solution and each area of uncertainty, where $Q_{\min} \leq Q \leq Q_{\min}+1.5$) of focal mechanism solution of these earthquakes determined only by initial motion polarity of P waves is less than 0.1π for all axes. I re-determined the focal mechanism solution of these earthquakes with initial motion polarity of S waves in addition to those of P waves, within the above area of uncertainty. By assuming that the initial motion polarity estimated by the focal mechanism solution is the theoretical value, and comparing the observed initial motion polarity with this, I investigated to what degree these values were consistent with each other. When I observed the initial

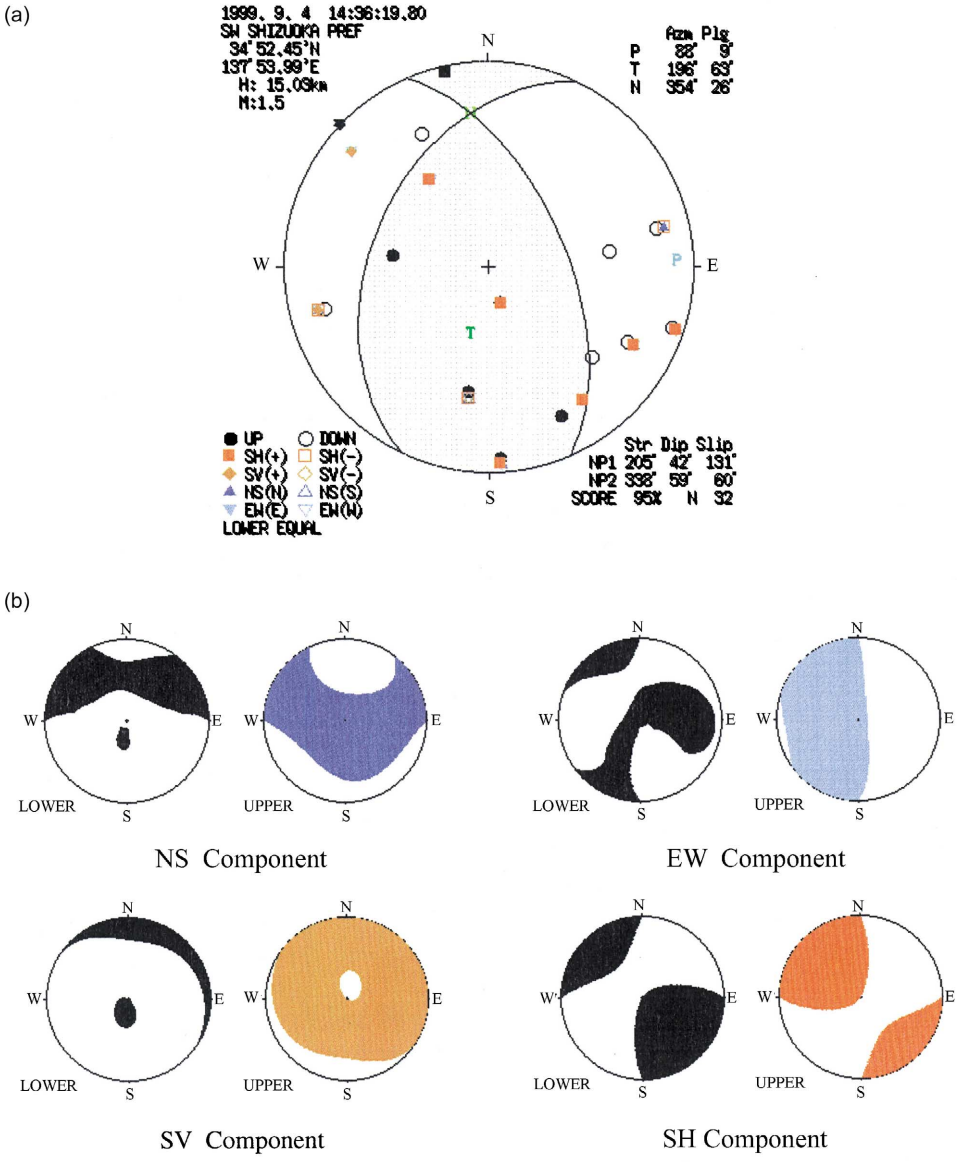

Fig. 5. (a) The focal mechanism solution of the earthquake, which occurred southwest of Shizuoka prefecture on 4 September 1999. In the upper left, origin time, region name of the epicenter, epicenter, focal depth, and magnitude are shown. In the lower left, the definition of symbols that distinguish the initial motion polarity and others are shown. In the upper right, focal mechanism solution (azimuth and plunge of P, T, and N axes) is shown. In the lower right, focal mechanism solution (strike, dip angle, and slip angle of two nodal planes), weighted score (degree of agreement between the theoretical value and the observed value of the initial motion polarity), and the weighted number of the observation stations are shown. In the case of observation stations where the initial motion polarity of S wave is observed, observation stations, for which seismic wave radiates from the hypocenter upward, are plotted in color other than black, the others are plotted in black. (b) The radiation pattern of the initial motion polarity of S wave. I show the radiation pattern (solid area is for N, E, and plus, respectively) of the initial motion polarity of S wave for NS component in the upper left, for EW component in the upper right, for SV component in the lower left, and for SH component in the lower right, respectively. The left one in each figure shows the case where seismic wave radiates from the hypocenter downward, and the right one shows the case where the radiation is upward.

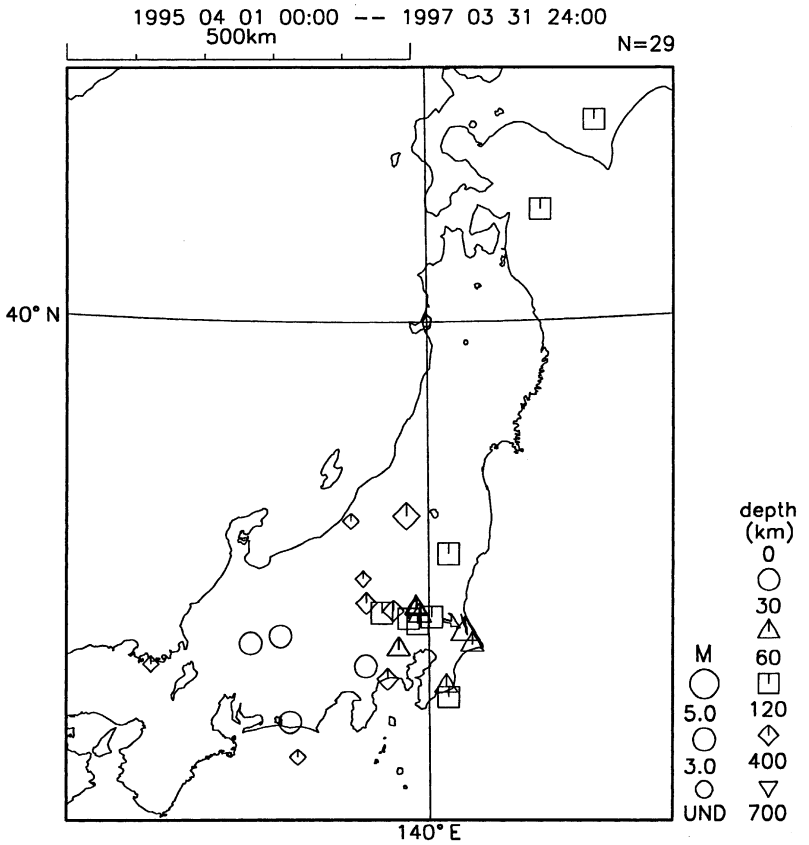

Fig. 6. Earthquakes whose mechanism solution is determined much stably only with the initial motion polarity of P waves. Depth of earthquakes is distinguished by symbol, and magnitude by size of the symbol.

motion polarity of S waves, I used the data of seismic waves observed by ground-based seismographs of JMA Urgent Earthquake and Tsunami Detection Network (T System), which are simply available. In Fig. 7, examples of waveforms (displacement waveforms made by integrating velocity waveforms, the earthquake occurred west of Fukushima prefecture on 4 December 1996) around the arrival time of the S wave are shown. The result is shown in Table 1.

Table 1 shows that the degree of agreement between the theoretical value and the observed value of the initial motion polarity of S waves exceeds 80% for all components, and that they are consistent with each other.

The number of the observed initial motion polarity data of S waves is about 100 for each component, so I can not make sure of the judgement whether the degree of agreement for SH component is significantly higher

Table 1
Degree of agreement between the theoretical values and the observed values of the initial motion polarity

	P wave (all data)	P wave (T system)	S wave (NS)	S wave (EW)	S wave (SV)	S wave (SH)
Consistent no.	1820	847	100	96	70	101
Total no.	1899	875	124	115	87	117
Rate (%)	96	97	81	83	80	86

T system: JMA Urgent Earthquake and Tsunami Detection Network.

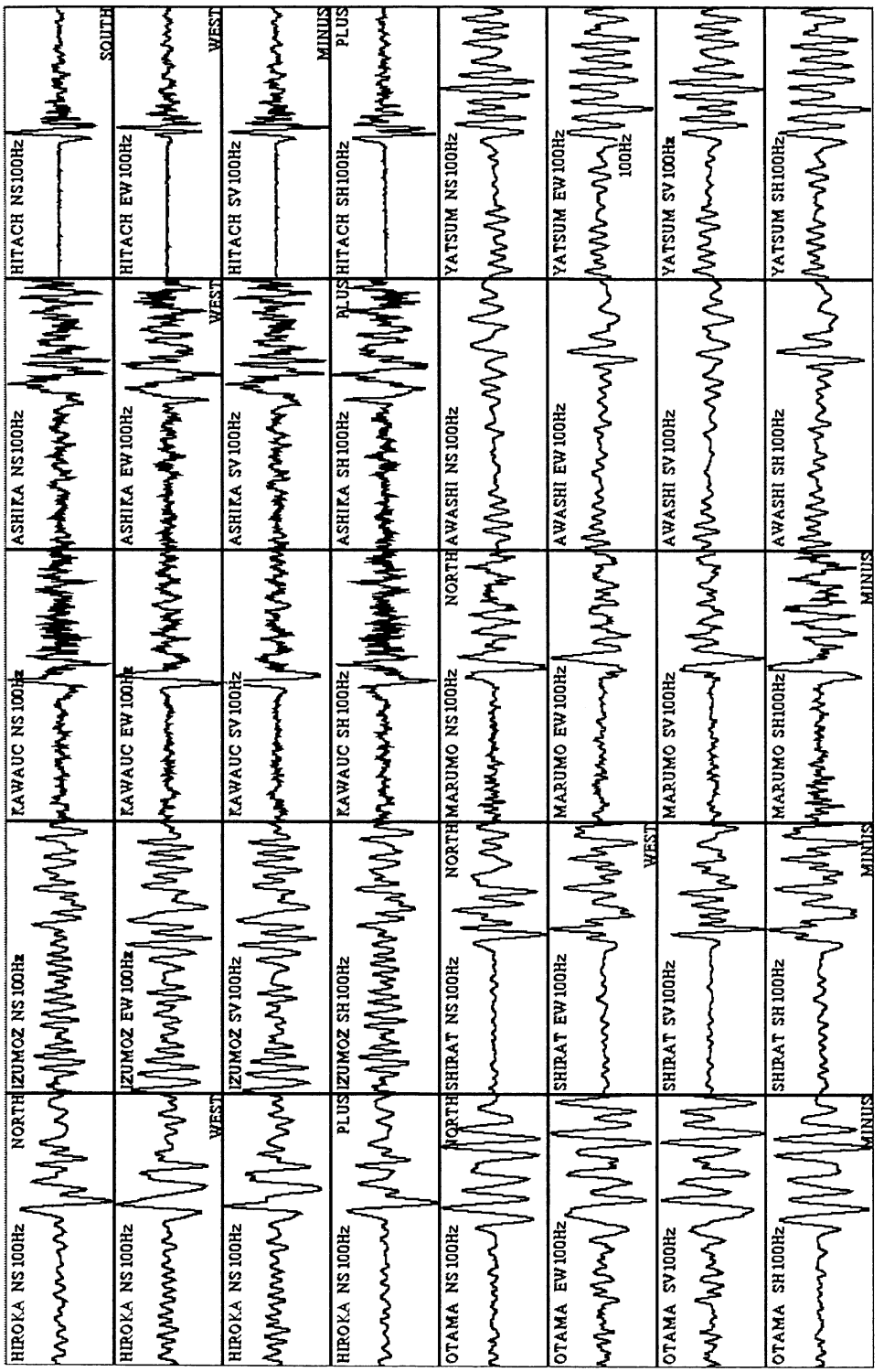

Fig. 7. Examples of waveforms near the S wave arrival time. The earthquake occurred west of Fukushima prefecture on 4 December 1996. These are displacement waveforms obtained by integrating the velocity waveforms. I show the name of the observation station, the name of the component and others in the upper left of each waveform, and show the observed value in the right hand side in the case of the waveform on which I observed the initial motion polarity.

than that for others or not. However, the reason why the degree of agreement for SH component is higher than that for others, is considered that SV component includes those converted from P waves, so that the possibility of misinterpretation is higher for NS and EW components, which are compounded from SH and SV components, in addition to SV components.

From the investigation result shown in Table 1, it is considered that W_i of S waves from 0.9 to 0.85 is adequate when that of P waves is 1.0. In this article, W_i of P waves is 1.0, that for SH component of S waves is 0.9, and W_i for other components of S waves is 0.85. Moreover, it is necessary that summation of W_i's for initial motion polarity data of all components of S waves per observation station is 2.0 at most, in order not to give an excessive weight value to that of S waves.

Fig. 5(b) shows that the radiation pattern of the initial motion polarity of S waves is markedly different from that of P waves. For this reason, it is expected that we can determine the focal mechanism solution for the earthquakes which occur in the area of low observation station density, or in the area where the distribution of observation station is biased, or for the earthquakes whose magnitude is small or micro, with sufficient accuracy, by using the initial motion polarity of S waves in addition to that of P waves. The examples of analysis for such a case are as follows.

Fig. 8 shows the example of analysis of the earthquake which occurred near Amami Oshima in Japan, which is the area where the number of observation stations is small, and the distribution of them is strongly biased. Fig. 8(a) shows the focal mechanism solution, Fig. 8(b) shows the area of uncertainty (where $Q_{\min} \leq Q \leq Q_{\min} + 1.5$: same in the rest of this section) for P and T axes, and Fig. 8(c) shows the area of uncertainty for P and T axes when the focal mechanism solution is determined only by the initial motion polarity of P waves. Moreover, Table 2 shows the reliability

Table 2
The reliability of focal mechanism solution of the earthquake which occurred near Amami Oshima on 22 April 1996

	P axis	T axis	N axis	A axis	B axis
Reliability					
P and S	0.34	0.20	0.37	0.20	0.36
Only P	0.50	0.49	0.50	0.46	0.50

Unit: π radian.

Table 3
The reliability of focal mechanism solution of the earthquake which occurred southwest of Shizuoka Prefecture on 4 September 1999

	P axis	T axis	N axis	A axis	B axis
Reliability					
P and S	0.13	0.30	0.31	0.28	0.22
Only P	0.32	0.50	0.50	0.45	0.33

Unit: π radian.

(maximum center angle between each axis of the focal mechanism solution and each area of uncertainty) for each axis of focal mechanism solution in the case using only the initial motion polarity of P waves and the case using that of S waves in addition to that.

Furthermore, Fig. 9 shows the example of analysis of the micro earthquake (M:1.5), which occurred southwest of Shizuoka prefecture in Japan. Fig. 9(a) shows the focal mechanism solution and Fig. 9(b) the area of uncertainty for P and T axes. In Fig. 9(c), the area of uncertainty for P and T axes is shown when the focal mechanism solution is determined only by initial motion polarity of P waves. Moreover, Table 3 shows the reliability for each axis of the focal mechanism solution in the case using only the initial motion polarity of P waves and the case using that of S waves in addition to this.

These examples of analysis show that the reliability for each axis of the focal mechanism solution improves by using the initial motion polarity of S waves in addition to that of P waves. In this way, by using this method, we can determine the focal mechanism solution for the earthquakes which occur in the area of low observation station density, or in the area where the distribution of observation station is biased, or for the earthquakes whose magnitude is small or micro, more accurately than the conventional method.

The spacing among stations in the earthquake observation network southwest of Shizuoka Prefecture where the earthquake, analyzed in Fig. 9, occurred, is as short as the inter-station intervals of the Japanese nationwide earthquake observation network which will be accomplished in the near future. Moreover, judging from the examples of waveforms around the arrival time of the S wave shown in Fig. 7, it is easy to identify the initial motion polarity of S waves as well as that of P waves. These suggest that this method

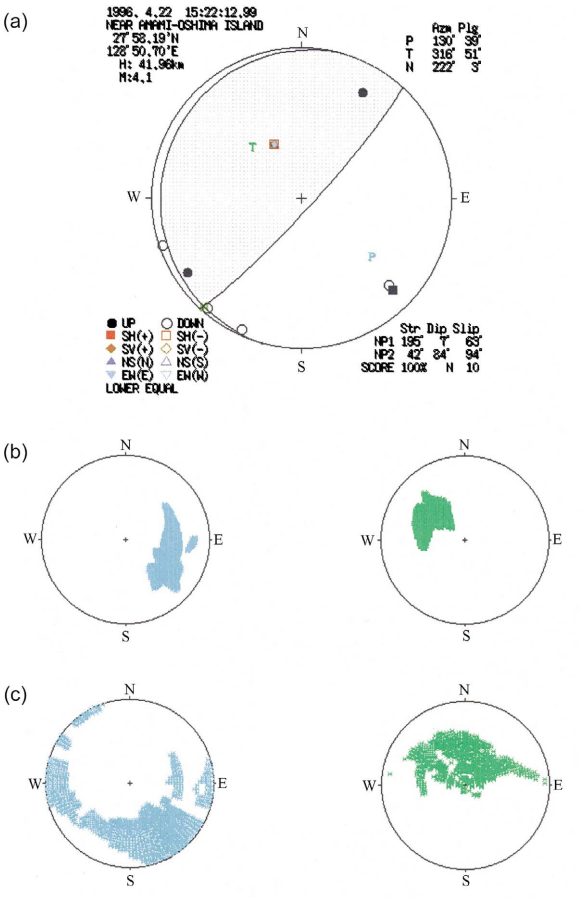

Fig. 8. (a) Focal mechanism solution of the earthquake which occurred near Amami Oshima on 22 April 1996. (b) Area of uncertainty (where $Q_{\min} \leq Q \leq Q_{\min} + 1.5$) of P (left) and T (right) axes in the case of determining the focal mechanism solution by initial motion polarity of S waves in addition to that of P waves. (c) Area of uncertainty in the case of determining it only by that of P waves. In the case of (c), I calculated the solution in the mesh larger than in the case of (b), because the area of uncertainty is wide.

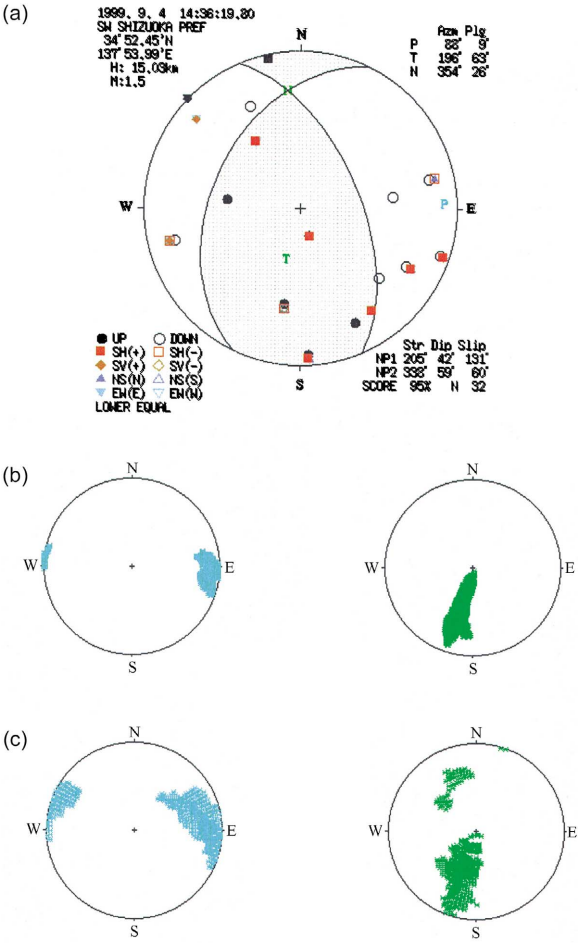

Fig. 9. (a) Focal mechanism solution of the earthquake which occurred southwest of Shizuoka prefecture on 4 September 1999 (same as Fig. 5(a)). (b) Area of uncertainty for each axis in the case of determining the focal mechanism solution by the initial motion polarity of S waves in addition to that of P waves. (c) Area of uncertainty in the case of determining it only by the initial motion polarity of P waves.

is adequate to apply routinely to earthquakes which occur all over Japan.

Generally, the initial motion polarity of S waves is not clear, and how easily we can identify it depends on the character of the target earthquake, the path along which the seismic wave travels, and the site effect near the observation station. We can roughly estimate how many initial motion polarity data of S waves we can interpret by comparing the size of the initial motion polarity data of P waves observed by T system and that of S waves, shown in Table 1. Table 1 shows that the size of the observed values of initial motion polarity of S waves per each component is from 10 to 15% of that of P waves. However, in some cases, we can identify the initial motion polarity of S waves for each component as many as that of P waves, for example, in the case of the earthquake shown in Fig. 9 (the size of observed value of initial motion polarity

of P waves is 12, that of S waves for NS component is 7, that for EW component 10, that for SV component 8, and that for SH component 10). It is necessary to investigate additionally how effective this method is for every region where earthquakes occur.

In this study, I use the displacement waveforms, which are obtained by numerically integrating the velocity waveforms, when I deal with the initial motion polarity of S waves. Because it is easier to identify it by displacement waveforms than by raw velocity waveforms, and the degree of agreement between the theoretical values and the observed values shown in Table 1 becomes higher. This know-how came experientially in the process of this study, and it can not be judged which is important the effect of high cut filtering by integral or the data are treated as displacement waveforms.

By the way, it is considered that there are some possibilities to misidentify the initial motion polarity of S waves because of S wave splitting. Therefore, it is necessary not to identify it for the observation station where we can observe S wave splitting because of the anisotropy around the station. Fig. 10 shows the case where we misidentify the initial motion polarity of S waves because of S wave splitting, that is, the case where an axis perpendicular to the vector component, for which we try to observe it, exists in the acute angle θ between the oscillation direction of the S wave when splitting does not occur and the direction for which the velocity of the S wave is higher. When these directions are given at random, the probability of the misidentification is 50% in the case of $\theta = 90^\circ$, it is 0% in the case of $\theta = 0^\circ$, and it becomes 25% on the average. Moreover, when the amplitude of initial motion of the S wave is X when no splitting occurs, and when the amplitude of initial motion of the split S wave is Y, then $Y = X\cos\theta$, so Y is approximately 0 in the neighborhood of $\theta = 90^\circ$. Therefore, this probability is expected to become lower. When the problematic area of anisotropy is relatively small, that is, when only a part of the observation stations is affected, there is little problem because the analysis has the effect of averaging. Even when the problematic area of anisotropy affects relatively many observation stations, there will be little problem if we use SH or SV component for identification and the epicenter is surrounded by observation stations, whose relative direction with respect to the epicenter varies with the observation stations.

In this article, $\epsilon = 1.5$ is used experientially, when I evaluate the reliability of the focal mechanism solution. It is necessary to investigate separately the theoretical basis which gives the value of ϵ. However, in such a case where we treat the focal mechanism

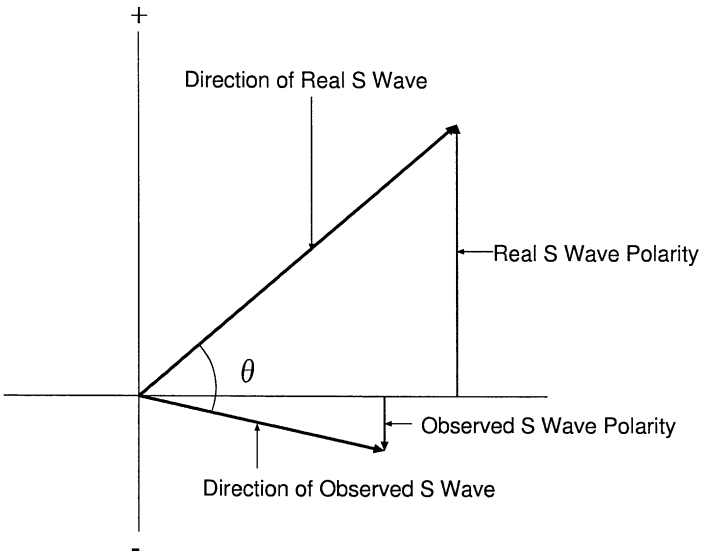

Fig. 10. The influence of S wave splitting to initial motion polarity of S waves. In this case, we misidentify the initial motion polarity of S waves because of S wave splitting.

solution of many earthquakes statistically, for example, when we evaluate the crustal stress field in the area where earthquakes occurred, it is enough to evaluate the reliability of focal mechanism solution by maximum center angle between each axis of focal mechanism solution and each area of uncertainty, where $Q_{\min} \leq Q \leq Q_{\min} + \epsilon$ is searched for each axis of solution over the focal sphere, taking the value of ϵ into account.

4. Conclusion

When we determine the focal mechanism solution by seismograms recorded by high sensitivity seismographs, we can improve the accuracy by using the initial motion polarity of S waves in addition to that of P waves. This method is adequate to apply routinely to determine the focal mechanism solution of earthquakes which occur all over Japan where we will have a nationwide earthquake observation network of high sensitivity seismographs at a few tens of kilometers interval in the near future.

Moreover, it is adequate to express the reliability of focal mechanism solution by maximum center angle, viewed from the center of the focal sphere, between the solution and the area where $Q_{\min} \leq Q \leq Q_{\min} + 1.5$ is searched for each axis of solution over focal sphere.

Acknowledgements

I would like to express my gratitude to Dr. S. Horiuchi in National Research Institute for Earth Science and Disaster Prevention (NIED), Dr. A. Yoshida, Dr. H. Ito, Dr. M. Hoshiba, Dr. Y. Yoshida, and ex-director Dr. K. Horai in Meteorological Research Institute for valuable discussions. I also thank members of JMA, Tokyo University, Nagoya University and NIED, who operate the routine observation network, for providing valuable data in this study. I appreciate the valuable comments and the reviews of the editors and anonymous referees, who helped to improve this manuscript.

References

Aki, K., Richards, P.G., 1980. Quantitative seismology: theory and method. Freeman, New York, pages 115 and 140–141.

Hamada, N., 1984. Re-examination of travel time tables for local earthquakes. Papers in Meteorology and Geophysics 35, 109–167 (in Japanese, with English abstract).

Hirasawa, T., 1970. Focal mechanism determination from S wave observations of different quality. J. Phys. Earth 18, 285–294.

Ito, Y., Ito, A., Hasegawa, A., Kasahara, M., 1998. Focal mechanisms of microearthquakes in Nikko–Ashio region, Japan, using short period body wave inversion. In: Prceedings of the Japan Earth and Planetary Science Joint Meeting on The Abstracts 1998, p. 295 (in Japanese).

Julian, R.B., Foulger, G.R., 1996. Earthquake mechanism from linear-programming inversion of seismic-wave amplitude ratios. Bull. Seismol. Soc. Am. 86, 972–980.

Kisslinger, C., 1980. Evaluation of S to P Amplitude ratios for determining focal mechanisms from regional network observations. Bull. Seismol. Soc. Am. 70, 999–1014.

Nakamura, A., Horiuchi, S., Hasegawa, A., 1999. Joint focal mechanism determination with source-region station corrections using short-period body-wave amplitude data. Bull. Seismol. Soc. Am. 89, 373–383.

Nakamura, M., Mochizuki, E., 1988. Focal mechanism solutions and their reliability determined by P wave first motions. Q. J. Seismol. 52, 1–14 (in Japanese, with English abstract).

Rau, R., Wu, F.T., Shin, T., 1996. Regional network focal mechanism determination using 3D velocity model and SH/P amplitude ratio. Bull. Seismol. Soc. Am. 86, 1270–1283.

Snoke, J.A., Munsey, J.W., Teague, A.C., Bollinger, G.A., 1984. A Program for focal mechanism determination by combined use of polarity and SV–P amplitude ratio data. Earthquake Notes 55, 15.

Stauder, W.S.J., Bollinger, G.A., 1964. The S wave project for focal mechanism studies earthquakes of 1962. Bull. Seismol. Soc. Am. 54, 2199–2208.